

On Frank-Wolfe Optimization for Adversarial Robustness and Interpretability

Theodoros Tsiligkaridis, Jay Roberts
 Massachusetts Institute of Technology Lincoln Laboratory
 244 Wood St, Lexington, MA 02421
 {ttsili, jay.roberts}@ll.mit.edu

Abstract

Deep neural networks are easily fooled by small perturbations known as adversarial attacks. Adversarial Training (AT) is a technique that approximately solves a robust optimization problem to minimize the worst-case loss and is widely regarded as the most effective defense against such attacks. While projected gradient descent (PGD) has received most attention for approximately solving the inner maximization of AT, Frank-Wolfe (FW) optimization is projection-free and can be adapted to any L^p norm. A Frank-Wolfe adversarial training approach is presented and is shown to provide as competitive level of robustness as PGD-AT without much tuning for a variety of architectures. We empirically show that robustness is strongly connected to the L^2 magnitude of the adversarial perturbation and that more locally linear loss landscapes tend to have larger L^2 distortions despite having the same L^∞ distortion. We provide theoretical guarantees on the magnitude of the distortion for FW that depend on local geometry which FW-AT exploits. It is empirically shown that FW-AT achieves strong robustness to white-box attacks and black-box attacks and offers improved resistance to gradient masking. Further, FW-AT allows networks to learn high-quality human-interpretable features which are then used to generate counterfactual explanations to model predictions by using dense and sparse adversarial perturbations.

1. Introduction

Deep neural networks (DNN) are powerful models that have achieved excellent performance across various domains [20] by exploiting hierarchical representations of data. As these models are being deployed across industries, such as healthcare and autonomous driving, robustness and interpretability concerns become increasingly important. Several organizations have also identified important principles of artificial intelligence (AI) that include notions of reliability and transparency [29, 25, 22].

One issues of such large capacity models is that small,

carefully chosen input perturbations, known as adversarial perturbations, can lead to incorrect predictions [13]. Various enhancement methods have been proposed to defend against adversarial perturbations [18, 33, 24, 26]. One of the best performing algorithms is adversarial training (AT) [24], which is formulated as a robust optimization problem [37]. Computation of optimal adversarial perturbations is NP-hard [43] and approximate methods are used to solve the inner maximization. The most popular approximate method that has been proven to be successful is projected gradient descent (PGD). Training against weaker attacks can reduce the computational cost but leads to strong robustness against weak attacks and brittleness against stronger attacks. This can be due to gradient obfuscation [40, 3], a phenomena where networks learn to defend against gradient-based attacks by making the loss landscape highly non-linear. Another sign of gradient obfuscation is when adversarial attacks computed with a few iterations fail but black-box attacks successfully find adversarial perturbations [40, 14]. Frank-Wolfe (FW) optimization has been recently proposed in [8] and was shown to effectively fool standard networks with less distortion.

Another major concern is interpretability of DNN decisions and explanation methods for AI system users or stakeholders. Insights into model behavior based on counterfactual explanations has the potential to be very useful for users [41]. However, standard networks do not have interpretable saliency maps and adversarial attacks tend to be visually imperceptible. Some popular explanation methods include layerwise relevance propagation (LRP) [4], locally interpretable model-agnostic explanations [32], and contrastive explanations [9], but these methods only yield feature relevance and are susceptible to spurious correlations prevalent in standard networks [15]. The relationship between adversarial robustness and saliency map interpretability was recently studied in [11] but experiments were based on gradient regularization. Furthermore, recent works [39, 15] claim that existence of adversarial examples are due to standard training methods that rely on highly predictive but non-robust features, and make connections be-

tween robustness and explainability.

In this paper, we propose a Frank-Wolfe adversarial training method and empirically show that this approach of adversarial training achieves a high level of robustness against various types of strong attacks and combats gradient obfuscation for several architectures. Furthermore, improved interpretability is obtained and model predictions are explained using counterfactual reasoning [15]. Our main contributions are summarized below:

- An adversarial training method based on Frank-Wolfe (FW-AT) is presented that may be adapted for any L^p norm with minimal tuning parameters and remains projection-free.
- Theoretical guarantees are derived to relate the local geometry of the loss to the magnitude of the FW adversarial perturbation in the L^∞ norm case. Specifically it is shown that more locally linear loss landscapes tend to yield higher L^2 distortions despite achieving nearly the same L^∞ distortion. It is empirically shown that FW-AT achieves larger L^2 distortion for robust models than standard models despite having similar strength L^∞ attack.
- It is shown that FW-AT achieves high adversarial robustness similar to PGD-AT for a variety of architectures when evaluated against strong white-box attacks and a variety of black-box attacks demonstrating strong resistance to gradient masking.
- It is shown that counterfactual generated images obtained using FW can be used to explain model predictions by generating dense and sparse adversarial perturbations.

2. Background and Previous Work

Consider $(x_i, y_i) \sim \mathcal{D}$ pairs of data examples drawn from distribution \mathcal{D} . The labels span C classes. The neural network function $f_\theta(\cdot)$ maps input features into logits, where θ are the model parameters. The class probability scores are obtained using the softmax transformation $p_c(x) = e^{f_{\theta,c}(x)} / \sum_l e^{f_{\theta,l}(x)}$. The predicted class label is given by $\hat{y}(x) = \arg \max_c f_{\theta,c}(x)$.

2.1. Adversarial Robustness

The prevalent way of training classifiers is through empirical risk minimization (ERM):

$$\min_{\theta} \mathbb{E}_{(x,y) \sim \mathcal{D}} [\ell(x, y; \theta)] \quad (1)$$

where the loss is the cross-entropy loss function given by $\ell(f_\theta(x), y) = \ell(x, y; \theta) = -y^T \log(p_\theta(x))$ and y denotes the one-hot label vector.

Adversarial robustness for a classifier f_θ is defined with respect to a metric, here chosen as the L^p metric associated with the ball $B_p(\epsilon) = \{\delta : \|\delta\|_p \leq \epsilon\}$, as follows. A network is said to be robust to adversarial perturbations of size ϵ at a given input example x iff $\hat{y}(x) = \hat{y}(x + \delta)$ for all $\delta \in B_p(\epsilon)$, i.e., if the predicted label does not change for all perturbations of size up to ϵ . The ϵ is often referred to as the strength or budget of the attack.

Training neural networks using the ERM principle (1) gives high accuracy on test sets, but leaves the network vulnerable to adversarial attacks. One of the most effective defenses against such attacks is adversarial training (AT) [24] which aims to minimize the adversarial risk instead,

$$\min_{\theta} \mathbb{E}_{(x,y) \sim \mathcal{D}} \left[\max_{\delta \in B_p(\epsilon)} \ell(x + \delta, y; \theta) \right]. \quad (2)$$

The training procedure constructs adversarial attacks at given inputs x that solve the inner maximization problem. Common maximization methods typically use a fixed number of gradient-ascent steps. One such method is projected gradient descent (PGD) that performs the iterative updates:

$$\delta^{(k+1)} = P_{B_p(\epsilon)} \left(\delta^{(k)} + \alpha \nabla_{\delta} \ell(x + \delta^k, y; \theta) \right) \quad (3)$$

where $P_{B_p(\epsilon)}(z) = \arg \min_{u \in B_p(\epsilon)} \|z - u\|_2^2$ denotes the orthogonal projection onto the constraint set. The sign of the gradient has also been shown to be an effective perturbation. The computational cost of this method is dominated by the number of steps used to approximate the inner maximization, since an K step PGD approximation to the maximization involves K forward-backward propagations through the network. While using fewer PGD steps can lower this cost, these amount to weaker attacks which can lead to gradient obfuscation [28, 40].

Prior works on regularization for adversarial robustness include gradient [23, 33] and curvature [26] regularization. Gradient regularization has not been shown to yield good robustness against strong attacks, while the relationship between small curvature and high robustness has been better established, but still leaves significant room for improvement. Based on the connection between curvature and robustness, a regularizer that promotes local linearity near training examples was proposed in [30] that is based on an iterative method leading to similar computational cost as PGD-AT. These methods argue that flattening the decision boundary via the loss is a suitable defense against adversarial attacks. Many defenses have been shown to be evaded by newer attacks while adversarial training has been demonstrated to maintain state-of-the-art robustness [3]. We develop a Frank-Wolfe adversarial training approach that is competitive with PGD-AT while offering increased transparency including an analytical expression for adversarial perturbations and distortion analysis that relates to the local loss geometry.

2.2. Counterfactual Explanations

Explanation methods based on counterfactual reasoning have been proposed in [41] and have the potential for end-to-end integrated use. Counterfactual explanations seek to provide the minimal amount of change in order to change a prediction. In particular, given an input x and distance metric d , a counterfactual explanation c is obtained by solving

$$\min_c d(x, c) \text{ s.t. } \hat{y}(x) \neq \hat{y}(c) \quad (4)$$

where \hat{y} denotes the prediction. Several works have studied finding nearest-neighbors of an input example that has a different prediction [27, 17]. Changing the prediction of a standard model in image space leads to imperceptible adversarial perturbations. For this reason, several works for visual counterfactual generation are based on generative models [34, 7]. However robust models themselves have been shown to change decisions when class-specific feature emerge in the image [39], which is needed to obtain human-interpretable counterfactuals. We demonstrate that our Frank-Wolfe framework is able to generate dense and sparse counterfactual perturbations to explain decisions.

3. Frank-Wolfe Adversarial Training

PGD-AT trains models on the worst case loss and requires careful tuning of the step size. It has been noted that choosing the step size α too small results in attacks which require many steps and choosing it too large leads to low robustness. This iterative method with large enough step size leaves the constraint set several times and may overshoot leading to suboptimal adversarial examples [42]. The generated adversarial examples tend to be on the boundary of the constraint set and have large distortion [8].

These observations lead us to consider a Frank-Wolfe (FW) optimization algorithm [12, 16]. This method is based calling a Linear Maximization Oracle (LMO) at each iteration, which makes it projection-free,

$$LMO = \bar{\delta}^k = \operatorname{argmax}_{\delta \in B_p(\epsilon)} \langle \delta, \nabla_{\delta} \ell(x + \delta^k, y) \rangle.$$

The LMO can be recognized as optimizing a linear approximation to the loss over the constraint set. After calling LMO, FW stakes a step using a convex combination with the current iterate,

$$\delta^{k+1} = \delta^k + \gamma^k (\bar{\delta}^k - \delta^k)$$

where $\gamma^k \in [0, 1]$ is the step size. While step sizes chosen using a backtracking line search or optimizing quadratic smoothness bounds can guarantee monotonic iterates, these require further computation which can be expensive for DNNs. In practice FW tends to require minimal tuning for the step size (in most cases γ^k is chosen as $c/(c+k)$ for

$c \geq 1$), while PGD performance strongly depends on step size. For our comparisons, we tune it to $c\epsilon/K$ for K -step PGD (PGD(K)) with $c > 1$ to ensure the boundary of the ball can be reached and allow movement on the boundary.

For general non-convex constrained optimization, the gradient norm is no longer an appropriate convergence criterion, and the Frank-Wolfe gap [12] is chosen instead:

$$g(\delta^k) = \max_{\delta \in B_p(\epsilon)} \langle \delta - \delta^k, \nabla_{\delta} \ell(x + \delta^k, y) \rangle \quad (5)$$

In general $g(\delta^k) \geq 0$ and δ^k is a stationary point if and only if $g(\delta^k) = 0$. Since the FW method calls the LMO oracle, a loss improvement proportional to the FW gap is expected, i.e.,

$$\ell(x^{k+1}, y) \approx \ell(x^k, y) + \gamma^k g(\delta^k) \quad (6)$$

where $x^k = x + \delta^k$. The approximate bound (6) implies that progress in the loss can be directly linked to the step size and the FW gap (5).

3.1. Closed-form solution to LMO

The FW sub-problem can be solved exactly for any L^p and the optimal $\bar{\delta}^k$ is given by

$$\bar{\delta}_i^k = \epsilon \phi_p(\nabla \ell_i^k) = \epsilon \begin{cases} \operatorname{sgn}(\nabla \ell_i^k) e_{i_k}^*, & p = 1 \\ \operatorname{sgn}(\nabla \ell_i^k) \frac{|\nabla \ell_i^k|^{q/p}}{\|\nabla \ell_i^k\|_q^{q/p}}, & 1 < p < \infty \\ \operatorname{sgn}(\nabla \ell_i^k), & p = \infty \end{cases} \quad (7)$$

where $\nabla \ell = \nabla_{\delta} \ell(x + \delta^k, y)$ and $1/p + 1/q = 1$. For $p = 1$, $i_k^* = \operatorname{argmax}_i |\nabla \ell_i^k|$ and $e_{i_k}^*$ is the canonical basis vector that is equal to 1 for the i_k^* -th component and zero otherwise.

FW does not require a projection onto the L^p ball which is non-trivial for p not in $\{2, \infty\}$. Interestingly, for the special case of L^∞ attacks the optimal solution becomes the signed gradient of the loss, i.e. $\bar{\delta}^k = \epsilon \operatorname{sgn}(\nabla_{\delta} \ell(x + \delta^k))$ which matches the Fast Gradient Sign Method (FGSM) of adversarial attacks [13].

3.2. Distortion Analysis for Robustness

Though all L^p attacks must remain in $B_p(\epsilon)$ their L^q norms, for $q \neq p$, can be quite different. This is referred to as distortion and in particular for L^∞ attacks we are interested in the L^2 distortion.

It has been empirically observed in recent work [8] that FW achieves a lower distortion than PGD attacks for standard networks while still achieving high success rates. Figure 1 (b) illustrates this empirically on three architectures trained with ERM (1) and AT (2) on CIFAR-10. We analyze the distortion of L^∞ FW(20) and PGD(20) attacks of strength $\epsilon = 8/255$ on the CIFAR10 test dataset. Robust

models were trained with PGD(10)-AT, but we note that the same behavior occurs for FW-AT robust models.

In Figure 1 (a) we see that in the case of standard models, FW has lower L^2 distortion than PGD adversarial attacks for almost all test images while still finding attacks that are near the L^∞ boundary (see bottom row of Figure 1 (b)). The first row of Figure 1 (b) shows that when attacking robust models both PGD and FW produce more distorted attacks. While this phenomenon is difficult to explain for PGD, Theorem 2 provides an explanation as to why FW attacks have more distortion when attacking robust versus standard models. First, an analytical expression for the FW-AT adversarial perturbation is derived in the following proposition.

Proposition 1. *The FW-AT Algorithm with step sizes $\gamma^k = c/(c+k)$ for some $c \geq 1$ yields the following adversarial perturbation after K steps*

$$\delta^K = \epsilon \sum_{l=0}^{K-1} \alpha^l \phi_p(\nabla_{\delta} \ell(x + \delta^l, y)) \quad (8)$$

where $\alpha^l = \gamma^l \prod_{i=l+1}^{K-1} (1 - \gamma^i) \in [0, 1]$ are non-decreasing in l , and sum to unity.

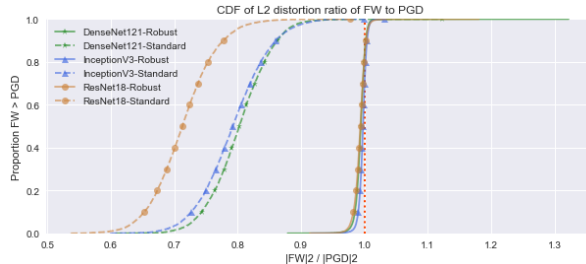
Proposition 2 shows that the FW adversarial perturbation may be expressed as a convex combination of the scaled loss gradients. Furthermore, for $c = 1$ all coefficients are uniform $\alpha^l = 1/K$ while larger $c > 1$ leads to a slower step-size decay and places more weight on later steps.

Theorem 1. *Consider the FW-AT Algorithm 1 with step sizes $\gamma^k = c/(c+k)$ for some $c \geq 1$ and the L^∞ norm case. Let $\cos \beta^{lj}$ be the directional cosine between $\text{sgn}(\nabla_{\delta} \ell(x + \delta^l, y))$ and $\text{sgn}(\nabla_{\delta} \ell(x + \delta^j, y))$. The magnitude of the adversarial perturbation δ^K is:*

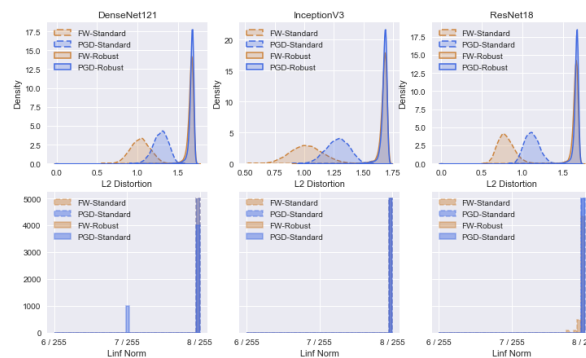
$$\begin{aligned} \|\delta^K\|_2 &= \epsilon \sqrt{d} \sqrt{1 - \sum_{l \neq j} \alpha^l \alpha^j (1 - \cos \beta^{lj})} \quad (9) \\ &= \epsilon \sqrt{d} \sqrt{1 - \frac{2}{d} \sum_{l \neq j} \alpha^l \alpha^j n^{lj}} \end{aligned}$$

where $\alpha^l = \gamma^l \prod_{i=l+1}^{K-1} (1 - \gamma^i)$ and n^{lj} is the number of sign changes between the gradients at $x + \delta^l$ and $x + \delta^j$.

Theorem 2 shows that the less aligned the signed gradients generated by the LMO at every step are, the smaller the L^2 distortion will be. Thus, it is expected that for standard networks which have highly nonlinear loss landscapes, the L^2 distortion will be small despite exhibiting high L^∞ distortion near ϵ . Robust models have a smoother loss landscape (see Figure 3) and so their gradients will change sign much less often during the attack leading to higher distortions. Such a distortion is not guaranteed by PGD and in



(a) CDF of FW vs PGD L^2 Distortions



(b) Density of L^2 Distributions and Histogram of L^∞ norms

Figure 1: L^∞ attacks using FW(20) and PGD(20) with $\epsilon = 8/255$ against standard (dashed) and robust (solid) models across three architectures. (a) The CDF of $\|\delta_{FW}\|_2 / \|\delta_{PGD}\|_2$. (b) Kernel density estimates (first row) of the L^2 distortion distribution and (second row) a histogram of the L^∞ norm of the attacks.

Figure 1 FW indeed produces higher distortion for robust models than standard ones. We believe this higher distortion is the force behind FW-AT achieving high robustness, particularly in the L^∞ regime. While both methods allow a model to be trained with strong L^∞ attacks, FW-AT offers more transparency in the adversarial training process. The proofs of Proposition 2 and Theorem 2 are in the supplementary.

3.3. Convergence Analysis

Loss functions $\ell(x + \delta, y)$ in deep neural networks are non-convex in general. For a targeted attack that aims to fool the classifier to predict a specific label, without loss of generality, we seek to minimize the loss $f(\delta) = \ell(x + \delta, y)$ over a L^p constraint set. The untargeted case follows similarly.¹ For general non-convex constrained optimization, the Frank-Wolfe gap given by (5) is non-negative in general and zero at stationary points. The convergence of FW on non-convex functions has been studied in [19] and recently improved for strongly convex constraints in [31].

¹For untargeted attacks, $\min_{\delta \in B(\epsilon)} -\ell(x + \delta, y)$ is considered and the FW gap becomes (5).

Consider the following smoothness assumption.

Assumption 1. *The function f has L -Lipschitz continuous gradients on $B_p(\epsilon)$, i.e., $\|\nabla f(u) - \nabla f(v)\| \leq L\|u - v\|, \forall u, v \in B_p(\epsilon)$.*

Assumption 1 is a standard assumption for the non-convex setting and has been made in several works [19, 8]. A recent study [36] shows that the batch normalization layer used in modern neural networks makes the loss much smoother. Other recent works [1, 45, 6] showed that the loss is semi-smooth for overparameterized DNNs. Furthermore, the process of adversarial training smooths the loss landscape in comparison to standard models significantly as Fig. 3 illustrates and other works have noted this phenomenon as well [26, 30].

Given Assumption 1 and the compactness of the constraint sets, all limit points of FW are stationary points [5]. The convergence rate of FW to a stationary point for optimization over arbitrary convex sets was first shown in [19] given by

$$\min_{1 \leq s \leq t} g(\delta_s) \leq \frac{\max\{2h_0, L \text{diam}(B)\}}{\sqrt{t+1}}$$

where $h_0 = f(\delta_0) - \min_{\delta \in B(\epsilon)} f(\delta)$ is the initial global suboptimality. It follows that larger ϵ imply a larger diameter and more iterations may be needed to converge². This result implies that an approximate stationary point can be found with gap less than ϵ_0 in at most $O(1/\epsilon_0^2)$ iterations. Theorem 4 in [31] shows that for smooth non-convex functions over strongly convex constraint sets, FW yields an improved convergence rate $O(\frac{1}{t})$, which importantly does not hold for the L^∞ constraint.

3.4. Algorithm

Algorithm 1 illustrates the Frank-Wolfe adversarial training method. The perturbation δ is initialized at zero or randomly initialized as $\delta \sim \mathcal{U}([- \zeta, \zeta]^d)$ for the L^∞ norm and $\delta = \zeta u / \|u\|_2, u \sim \mathcal{N}(0, I_d)$ for the L^2 norm, where $\zeta \in (0, \epsilon]$. In our experiments, we used zero initialization. The loss gradient is computed at each Frank-Wolfe iteration k , and the solution to the LMO $\bar{\delta}$ is given by (7). Then the adversarial perturbation δ is updated by taking a step along the direction $\bar{\delta} - \delta$. Once the adversarial examples are obtained, the model parameters θ are updated using a gradient-based optimizer (e.g. SGD).

3.5. Computational Complexity

Each step in the inner maximization based on the Frank-Wolfe procedure requires a forward-backward pass to evaluate $\nabla \ell(\cdot)$, similarly to PGD. Thus $O(KN_w)$ time is needed for K steps of FW where N_w denotes the number of

²The diameter of L^2 ball is 2ϵ and for the L^∞ ball $2\epsilon\sqrt{d}$.

network parameters. After computing the adversarial direction δ^* , the gradient-based optimizer incurs an additional cost of $O(N_w)$ for all methods to update model parameters.

Algorithm 1: Frank-Wolfe Adversarial Training

Input : Network f_θ , Training data \mathcal{D} , Training epochs T , max number of steps K , batch size $|B|$, maximum perturbation ϵ , constant $c \geq 1$, learning rate schedule η_t .

Output: Robust model θ .

```

1 for  $t = 0$  to  $T - 1$  do
2   for each batch  $(x, y) \sim \mathcal{D}$  do
3     Initialize  $\delta$  (zero/random)
4     while  $k < K$  do
5        $\gamma = c/(c + k)$ 
6        $\bar{\delta} = \epsilon \phi_p(\nabla_{\delta} \ell(f_\theta(x + \delta), y))$  (see (7))
7        $\delta = \delta + \gamma(\bar{\delta} - \delta)$ 
8     end
9      $\theta = \theta - \eta_t \frac{1}{|B|} \sum_{i \in B} \nabla_{\theta} \ell(f_\theta(x_i + \delta_i), y_i)$ 
10  end
11 end
```

4. Counterfactual Explanations

The framework of counterfactual explanation aims to explain individual model predictions by looking for the closest image from the original that will change the prediction [41]. Closely related explanation methods includes contrastive ones that describe how features will change the prediction if absent or present [21].

This framework can be used to answer user question types including ‘why not’ and ‘how to be that’. As an example consider a loan processing application that was denied, then counterfactual explanation could take the form ‘how would income and debt need to change to grant the loan?’. Counterfactual explanations are closely tied to human explanations and tie the classifier’s decision directly to the explanation, offering an advantage over feature attribution [4] or sensitivity-based [44] explanations. Although saliency maps for robust models focus identify semantically meaningful areas in the image that most influence the predictions [11], they cannot be directly used to reason about how feature changes can correct or justify a misclassification for instance.

To this end, we seek to generate visual counterfactuals in the image space by constraining the change in the original image. Our framework is inspired by robust feature manipulation [39] and the connection between the formulation of finding counterfactuals (4) and computing adversarial perturbations (10) [41, 38]. As the network’s prediction changes, class-specific features are expected to

emerge. Standard models do not achieve this as they make use of predictive but non-robust features and decisions are changed by imperceptible perturbations. Therefore, we consider explaining decisions of robust models that have shown to have generative properties [39, 35].

Suppose we have $(x, y) \sim \mathcal{D}$, counterfactual images are generated to explain model predictions as defined by the optimization problems

$$\delta_{\max} = \operatorname{argmax} \ell(x + \delta, y), \quad \delta_{\min} = \operatorname{argmin} \ell(x + \delta, y), \quad (10)$$

we optimize the loss over a L^p ball of radius ϵ to ensure that the modified example $x + \delta$ remains close to the original example x . For L^2 counterfactual perturbations δ are dense, and sparse counterfactual perturbations can be obtained by optimizing the loss using the sparsity-inducing L^1 norm instead. For correct predictions, δ_{\max} constructs a counterfactual image to explain how the correct prediction changes to an incorrect one, while δ_{\min} changes features to increase the confidence of the correct class. On the other hand, for incorrect predictions, δ_{\max} answers the counterfactual question of how features change to justify the incorrect label, and δ_{\min} shows feature changes to correct the error.

5. Experimental Results

We evaluate the performance of our proposed FW-based adversarial training (FW-AT) against standard training, and PGD-based adversarial training (PGD-AT) [24]. All networks were trained by fine-tuning a standard model.

5.1. Implementation

The models, training, and evaluation routines for our experiments were performed using the robustness library from [10] which we modified to add the FW-AT method and support the SVHN dataset. Experiments were run on 2 Volta V100 GPUs. Hyperparameters for FW-AT were tuned to $c = 2$ with the goal of achieving near the adversarial accuracy of PGD-AT with step size $\alpha = 2.5\epsilon/K$ for $K = 10$ steps as this was the default setting in [10]. Specifics can be found in the supplementary material.

5.2. Adversarial Robustness

To test the robustness of our network, we consider a variety of adversarial attacks, including white-box untargeted and targeted attacks towards a random class $r \sim \mathcal{U}(\{1, \dots, K\} \setminus y)$. The white-box setup considers attack techniques that have full access to the model parameters and are constrained by the same maximum perturbation size ϵ . The classification margin is defined as $M(x, y) = \log p_y(x) - \max_{j \neq y} \log p_j(x)$. The following white-box attacks are used for evaluating adversarial robustness:

(UL) Untargeted-loss: $\max_{\delta \in B(\epsilon)} \ell(x + \delta, y)$

Method	Clean	UL	TL	UM	TM
Standard	94.54	1.37	15.62	1.88	16.82
FW(10)-AT	89.41	65.62	85.12	65.92	84.49
PGD(10)-AT	89.46	65.44	84.97	65.72	83.94

(a) L^2 adversarial PGD(20) attacks with loss / margin at $\epsilon = 0.5$

Method	Clean	UL	TL	UM	TM
Standard	94.54	0.01	11.10	0.01	11.49
FW(10)-AT	84.37	47.86	74.37	46.56	72.41
PGD(10)-AT	84.12	47.75	75.30	46.83	72.45

(b) L^∞ adversarial PGD(20) attacks with loss / margin at $\epsilon = 8/255$

Table 1: Model accuracy on CIFAR-10 test set against various attacks on ResNet18 architecture. Our proposed FW-AT method has high robustness similar to PGD-AT.

(TL) Random Targeted-loss: $\max_{\delta \in B(\epsilon)} \ell(x + \delta, r)$

(UM) Untargeted-margin: $\min_{\delta \in B(\epsilon)} M(x + \delta, y)$

(TM) Random Targeted-margin: $\max_{\delta \in B(\epsilon)} M(x + \delta, r)$

The performance metric used is the accuracy on the test set after the attack is applied, i.e., adversarial accuracy. In general untargeted attacks are stronger than targeted ones. Table 1 reports robustness results on CIFAR-10 for the specific attacks in the L^2 and L^∞ cases respectively on ResNet18 architecture. FW-AT achieves robustness competitive with PGD-AT for untargeted and targeted attacks. Similar trends are shown on SVHN in the supplemental material (also Table 2). Additional results are shown on DenseNet121, InceptionV3, and ResNet50 architectures in Table 4.

5.3. Evaluating Gradient Masking

We evaluate gradient masking by following a similar evaluation protocol as in [26] inspired by [40]. Table 2 shows that our method achieves similar adversarial accuracy on the test set when evaluated against PGD attacks of increasing strength. Thus increasing the attack’s complexity does not deteriorate the adversarial accuracy significantly.

In the black-box setting, attacks have access to the inputs and output logits (partial or full) only. Our models are evaluated against black-box gradient-free methods that repeatedly perform queries to construct adversarial images including SimBA [14], SPSA [40] and Square attack [2]. Attack parameters can be found in the supplementary material. Table 3 contains the adversarial accuracy obtained under PGD(100) white-box attack and several black-box attacks against maximum norm trained robust FW and PGD models. It is evident that the proposed FW-AT defense achieves similar robustness to PGD-AT. Furthermore, while black-box attacks are in general less powerful than white-box ones, Square attack is by far the strongest that comes close to white-box robustness levels and is a strong gradient-free

Method	Clean	PGD(20)	PGD(40)	PGD(100)
CIFAR10 / L^2 FW(10)-AT	89.41	65.62	65.46	65.29
CIFAR10 / L^2 PGD(10)-AT	89.46	65.44	65.23	65.16
CIFAR10 / L^∞ FW(10)-AT	84.37	47.86	47.47	47.22
CIFAR10 / L^∞ PGD(10)-AT	84.12	47.75	47.35	47.21
SVHN / L^2 FW(10)-AT	94.63	70.02	69.68	69.51
SVHN / L^2 PGD(10)-AT	95.00	69.98	69.62	69.45
SVHN / L^∞ FW(10)-AT	94.23	57.36	56.74	56.42
SVHN / L^∞ PGD(10)-AT	94.41	54.46	53.32	52.88

Table 2: Model accuracy on CIFAR-10 (top set) and SVHN (bottom set) test set for untargeted loss (UL) adversarial L^2 (and L^∞) PGD attacks at $\epsilon = 0.5$ (and $\epsilon = 8/255$) for L^2 (and L^∞) robust networks trained on ResNet18 architecture. The step size was set to $\alpha = 2\epsilon/10$ ($= 0.1$ for L^2 and $= 1.6/255$ for L^∞). Our proposed method, FW-AT, achieves high adversarial accuracy and resistance to gradient masking similar to PGD-AT.

evaluation.

Figure 2 compares the margin computed using Square attack and PGD(100) attack for a large batch of test points. It is observed that both methods lead to a similar adversarial loss except on a very small subset of points (48 out of 1000) for FW-AT which improves upon the number of red points for PGD-AT (65 out of 1000). Here, the adversarial loss corresponds to the classification margin which captures the confidence in correct classifications and is positive for correct predictions and negative for misclassifications. The results in Tables 2, 3 and Fig. 2 further verify that our FW method improves the true robustness and does not suffer from gradient masking or obfuscation.

Adversarial accuracy results for a variety of additional architectures including DenseNet121, InceptionV3, and ResNet50, are shown in Table 4. In all experiments FW-AT achieves robustness competitive with PGD-AT building upon our empirical results on ResNet18.

5.4. Loss Landscape

It has been shown experimentally that many robust models, including AT and the geometric-regularization methods (e.g. CURE), have more regular loss landscapes than their non-robust counterparts [23, 33, 26, 30]. Figure 3 shows sample loss surfaces for a standard model, adversarial training with PGD(10), and our adversarial training FW(10). The white circle denotes the original image, and the red circle denotes the L^∞ adversarial perturbation at $\epsilon = 8/255$. One direction is the adversarial perturbation and the other is a random orthogonal direction. We observe that the loss surface of standard models is highly non-linear and the loss varies significantly in this small neighborhood. In particular the largest variation occurs in the adversarial direction. Figure 3 (b) and (c) demonstrate that robust models offer more resistance to such local loss variation and that the variation is primarily in the direction of the adversarial attack. These results suggest high resistance to gradient obfuscation.

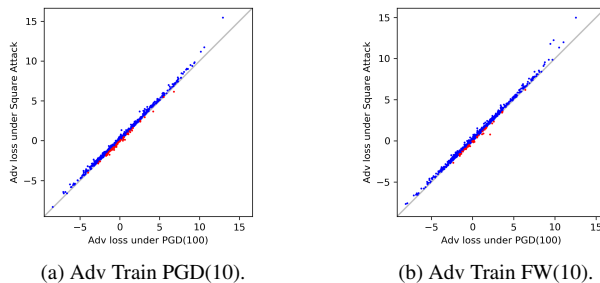


Figure 2: Gradient masking analysis for CIFAR10 PGD-AT and FW-AT L^∞ robust networks trained on ResNet18 architecture. Adversarial loss (classification margin) was computed with black-box Square Attack for the y-axis and white-box PGD(100) attack at $\epsilon = 8/255$ for x-axis on a set of 1000 test points. Points near the line $y = x$ indicate both types of attacks found similar adversarial perturbations, while points below the line shown in red imply that Square Attack identified stronger attacks than PGD. FW-AT exhibits a higher resistance to gradient masking.

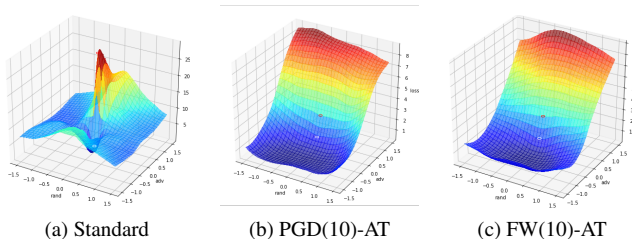


Figure 3: Loss landscapes for an image from CIFAR10 test set. ResNet18 architecture. Standard models have highly non-linear loss surfaces as opposed to robust models which have smoother landscapes.

Method	PGD(100)	SimBA	SPSA	Square
CIFAR10 / L^∞ FW(10)-AT	50.40	70.60	76.20	53.10
CIFAR10 / L^∞ PGD(10)-AT	49.10	70.40	75.50	52.20
SVHN / L^∞ FW(10)-AT	55.50	81.40	77.70	54.20
SVHN / L^∞ PGD(10)-AT	55.00	79.60	77.80	52.00

Table 3: Model accuracy on white-box PGD(100) and black-box (SimBA, SPSA, Square) attacks on CIFAR10/SVHN test subset (1000 examples) for L^∞ robust networks trained on ResNet18 architecture. The L^∞ attacks use $\epsilon = 8/255$. FW-AT maintains strong robustness against a variety of black-box attacks.

(Ar) Method	Clean	PGD(20)	PGD(100)	Square
(D) FW-AT	84.17	49.27	48.77	54.50
(D) PGD-AT	84.18	48.46	47.94	53.60
(I) FW-AT	85.45	47.40	46.88	53.00
(I) PGD-AT	85.52	47.50	47.10	53.30
(R) FW-AT	84.98	48.90	48.26	54.60
(R) PGD-AT	85.20	49.29	48.68	53.60

Table 4: Model accuracy on CIFAR10 test set for FW(10)-AT and PGD(10)-AT L^∞ robust networks trained on DenseNet121 (D), InceptionV3 (I) and ResNet50 (R) architectures. white-box PGD(20) UL attacks and black-box Square attacks (1000 examples) at $\epsilon = 8/255$.

5.5. Counterfactual Explanations

Figure 4 shows examples of the counterfactual explanations for two sample images from the CIFAR10 test set. The images’ target labels are ship and airplane. The model correctly classified the ship and misclassified the airplane as a ship. The explanations are generated by solving (10) in the dense case we restrict perturbations to the L^2 ball of radius 2 and use FW(20) and for the sparse case we restrict to the L^1 ball of radius of $255/4$ and use FW(768). The high number of steps is necessary as each Frank-Wolfe step in the L^1 optimization modifies at most one pixel at a time. FW(768) can modify at most 25% of the total pixels. Indeed the L^1 perturbations are sparse which can allow for more focused interpretations of the prediction, offering an advantage over PGD since projection onto the L^1 ball lacks a closed-form.

Consider the minimization perturbations (Figures 4a and 4c) for the correctly classified ship image (first column). The δ_{\min} perturbations show features that the model believes should be emphasized to become more confident in its correct prediction. The perturbations focus on the sail and seem to emphasize the water in the image. For the second column the δ_{\min} displays features that need to be added to correct the model’s misclassification of the airplane as a ship and the perturbations focus on the cockpit of the airplane and seem to add more of a traditional tail to the image.

The maximization perturbations (Figures 4b and 4d) for the correctly classified ship image (first column) show fea-

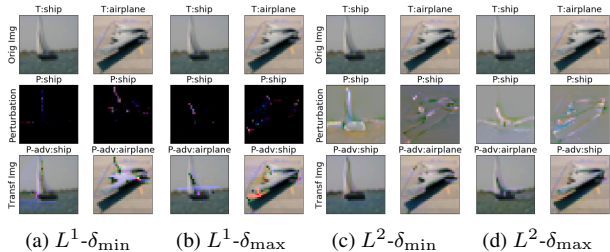


Figure 4: Sparse (a) and (b) and dense (c) and (d) counterfactual explanations via perturbations generated using (10). L^1 perturbations modified at most 25% of pixels with FW(768) and L^2 perturbations were performed with FW(20) and $\epsilon = 2$. Images are titled with their target label (T), the model’s prediction (P), and its adversarial prediction (P-adv).

tures of the image that could be emphasized to make a mistake. They emphasize the horizon to form wings and the mast to form a tail. For the second column δ_{\min} shows what features led to the model’s misclassification of the airplane as a ship. The sparse perturbations emphasize the wing tip while the L^2 model seems to blur the boundary overall making a perturbation which itself appears to be a ship.

6. Conclusion

One of the most effective defenses against adversarial perturbations is adversarial training (AT) under which networks are trained to be robust against worst-case perturbations computed using projected gradient descent (PGD). A Frank-Wolfe adversarial training approach (FW-AT) is presented and theoretical guarantees are derived to relate local loss geometry to the magnitude of FW adversarial perturbation for the L^∞ case, and it is shown that FW-AT achieves higher L^2 distortions for robust models than standard ones despite achieving nearly the same L^∞ distortion. It is empirically demonstrated to have high robustness competitive with PGD-AT against strong white-box attacks and black-box attacks, in addition to offering more resistance to gradient obfuscation. Visual counterfactual explanations are shown using FW dense and sparse perturbations.

Method	Clean	UL	TL	UM	TM
Standard	94.54	1.37	15.62	1.88	16.82
Gradient Reg	89.16	29.90	70.45	30.91	66.43
CURE	88.27	53.43	82.01	53.13	79.49
FW(10)-AT	89.41	65.62	85.12	65.92	84.49
PGD(10)-AT	89.46	65.44	84.97	65.72	83.94

(a) L^2 adversarial PGD(20) attacks with loss / margin at $\epsilon = 0.5$

Method	Clean	UL	TL	UM	TM
Standard	94.54	0.01	11.10	0.01	11.49
Gradient Reg	82.51	4.79	37.42	6.03	32.25
CURE	81.06	20.73	59.99	21.33	54.36
FW(10)-AT	84.37	47.86	74.37	46.56	72.41
PGD(10)-AT	84.12	47.75	75.30	46.83	72.45

(b) L^∞ adversarial PGD(20) attacks with loss / margin at $\epsilon = 8/255$

Table 5: Model accuracy on CIFAR-10 test set against various attacks. Our proposed method FW-AT outperforms prior gradient and curvature regularization methods and is competitive with PGD-AT.

Appendix

Training Details

Training. All robust models were trained starting from a pre-trained standard model. Training was performed for 61 epochs. A SGD optimizer was used with initial learning rate 0.01 and decayed to 0.001 after 50 epochs. The best model that achieves the highest adversarial accuracy on a heldout set is chosen in all experiments.

Hyperparameters

White box attacks. Our experiments are based on K -step PGD attacks with step size tuned to $\alpha = 2\epsilon/10$. This is equal to $\alpha = 0.1$ for the L^2 norm and $\alpha = 1.6/255$ for the L^∞ norm.

Black box attacks. The parameters used for the black-box attacks are the following: SimBA $T = 200$ iterations, $\epsilon = 0.2$, SPSA $T = 100$ steps, $B = 512$ batch size, $\epsilon = 8/255$ Square attack $T = 5000$ steps, $p_{init} = 0.8$, $\epsilon = 8/255$.

White Box Robustness Results

Tables 5 and 6 show the adversarial accuracy of FW-AT on CIFAR-10 and SVHN respectively, in comparison to standard training, PGD-AT [24], gradient regularization (Grad-Reg) [33], and curvature regularization (CURE) [26]. All networks were trained by fine-tuning the standard model. It is observed that FW-AT achieves similar robustness as PGD-AT on both datasets.

Method	Clean	UL	TL	UM	TM
Standard	97.04	9.77	30.09	10.00	30.54
Gradient Reg	95.00	46.39	76.48	47.15	74.43
CURE	94.68	63.78	86.29	63.33	84.66
FW(10)-AT	94.63	70.03	88.36	68.54	87.15
PGD(10)-AT	95.00	69.98	88.60	68.96	86.97

(a) L^2 adversarial PGD(20) attacks with loss / margin at $\epsilon = 0.5$

Method	Clean	UL	TL	UM	TM
Standard	97.04	0.51	12.75	0.52	13.36
Gradient Reg	91.42	6.10	29.01	7.13	26.04
CURE	91.61	30.36	59.25	29.79	54.69
FW(10)-AT	94.23	57.36	79.28	54.42	75.29
PGD(10)-AT	94.41	54.46	77.33	53.03	73.69

(b) L^∞ adversarial PGD(20) attacks with loss / margin at $\epsilon = 8/255$

Table 6: Model accuracy on SVHN test set against various attacks. Our proposed method FW-AT outperforms prior gradient and curvature regularization methods and is competitive with PGD-AT.

Proposition 2

The following proposition derives an analytical expression for the adversarial perturbation computed by FW-AT.

Proposition 2. *The FW-AT Algorithm with step sizes $\gamma^k = c/(c+k)$ for some $c \geq 1$ yields the following adversarial perturbation after K steps*

$$\delta^K = \epsilon \sum_{l=0}^{K-1} \alpha^l \phi_p(\nabla_{\delta} \ell(x + \delta^l, y)) \quad (11)$$

where $\alpha^l = \gamma^l \prod_{i=l+1}^{K-1} (1 - \gamma^i) \in [0, 1]$ are non-decreasing in l , and sum to 1.

Proof. The LMO solution is given by $\bar{\delta}^k = \epsilon \phi_p(\nabla_{\delta} \ell(x + \delta^k, u))$ and the update becomes

$$\begin{aligned} \delta^{k+1} &= \delta^k + \gamma^k (\bar{\delta}^k - \delta^k) \\ &= (1 - \gamma^k) \delta^k + \gamma^k \epsilon \phi_p(\nabla_{\delta} \ell(x + \delta^k, y)) \end{aligned}$$

Using induction on this relation yields after K steps:

$$\begin{aligned} \delta^K &= \delta^0 \prod_{l=0}^{K-1} (1 - \gamma^l) \\ &+ \epsilon \sum_{l=0}^{K-1} \gamma^l \prod_{i=l+1}^{K-1} (1 - \gamma^i) \phi_p(\nabla_{\delta} \ell(x + \delta^l, y)) \quad (12) \end{aligned}$$

where δ^0 is the initial point which affects both terms in (12) and $\gamma^k = c/(c+k)$ for $k \geq 0$. Since $\gamma^0 = 1$, the first term vanishes and (12) simplifies to

$$\delta^K = \epsilon \sum_{l=0}^{K-1} \alpha^l \phi_p(\nabla_{\delta} \ell(x + \delta^l, y)) \quad (13)$$

where the coefficients are

$$\alpha^l = \gamma^l \prod_{i=l+1}^{K-1} (1 - \gamma^i) \quad (14)$$

Since $\gamma^l \in [0, 1]$, it follows that $\alpha^l \in [0, 1]$. Induction on (14) yields that $\sum_{l=0}^{K-1} \alpha^l = 1$. Furthermore, $\alpha^l \leq \alpha^{l+1}$ follows from:

$$\begin{aligned} & \alpha^l \leq \alpha^{l+1} \\ \Leftrightarrow & \gamma^l (1 - \gamma^{l+1}) \leq \gamma^{l+1} \\ \Leftrightarrow & \frac{c}{c+l} \left(1 - \frac{c}{c+l+1}\right) \leq \frac{c}{c+l+1} \\ & \Leftrightarrow \frac{l+1}{c+l} \leq 1 \\ & \Leftrightarrow 1 \leq c \end{aligned}$$

Thus, the sequence α^l is non-decreasing in l . Since the coefficients sum to unity, (13) is in the convex hull of the generated LMO sequence $\{\phi_p(\nabla_{\delta^l} \ell(x + \delta^l)) : l = 0, \dots, K-1\}$. \square

Proof of Theorem 2

Theorem 2. Consider the FW-AT Algorithm with step sizes $\gamma^k = c/(c+k)$ for some $c \geq 1$ and the L^∞ norm case. Let $\cos \beta^{lj}$ be the directional cosine between $\text{sgn}(\nabla_{\delta^l} \ell(x + \delta^l, y))$ and $\text{sgn}(\nabla_{\delta^j} \ell(x + \delta^j, y))$. The magnitude of the adversarial perturbation δ^K is:

$$\begin{aligned} \|\delta^K\|_2 &= \epsilon \sqrt{d} \sqrt{1 - \sum_{l \neq j} \alpha^l \alpha^j (1 - \cos \beta^{lj})} \quad (15) \\ &= \epsilon \sqrt{d} \sqrt{1 - \frac{2}{d} \sum_{l \neq j} \alpha^l \alpha^j n^{lj}} \end{aligned}$$

where $\alpha^l = \gamma^l \prod_{i=l+1}^{K-1} (1 - \gamma^i) \in [0, 1]$ sum to unity and n^{lj} is the number of sign changes between the gradients at $x + \delta^l$ and $x + \delta^j$.

Proof. From Proposition 2, we obtain the following decomposition of the adversarial perturbation:

$$\delta^K = \epsilon \sum_{l=0}^{K-1} \alpha^l \text{sgn}(\nabla_{\delta^l} \ell(x + \delta^l, y))$$

To bound the magnitude of the adversarial perturbation, we have

$$\|\delta^K\|_2 = \sqrt{\|\delta^K\|_2^2} = \epsilon \sqrt{\left\| \sum_l \alpha^l s^l \right\|_2^2}$$

where we use the shorthand notation $s^l = \text{sgn}(\nabla_{\delta^l} \ell(x + \delta^l, y))$. The squared L^2 norm in the above is bounded as:

$$\begin{aligned} \left\| \sum_l \alpha^l s^l \right\|_2^2 &= \sum_l \sum_j \alpha^l \alpha^j \langle s^l, s^j \rangle \\ &= \sum_l (\alpha^l)^2 \|s^l\|_2^2 + \sum_{l \neq j} \alpha^l \alpha^j \|s^l\|_2 \|s^j\|_2 \cos \beta_{lj} \\ &= d \left(\sum_l (\alpha^l)^2 + \sum_{l \neq j} \alpha^l \alpha^j \cos \beta_{lj} \right) \\ &= d \left(\sum_l (\alpha^l)^2 + \sum_{l \neq j} \alpha^l \alpha^j - \sum_{l \neq j} \alpha^l \alpha^j (1 - \cos \beta_{lj}) \right) \\ &= d \left(1 - \sum_{l \neq j} \alpha^l \alpha^j (1 - \cos \beta_{lj}) \right) \end{aligned}$$

where we used $\|s^l\|_2 = \sqrt{d}$ and from Proposition 2 $(\sum_l \alpha^l)^2 = 1$. The final relation follows from the expansion of the squared difference of signed gradients:

$$\begin{aligned} \|s^l - s^j\|_2^2 &= \|s^l\|_2^2 + \|s^j\|_2^2 - 2 \langle s^j, s^l \rangle \\ &= \|s^l\|_2^2 + \|s^j\|_2^2 - 2 \|s^j\|_2 \|s^l\|_2 \cos \beta_{lj} \\ &= d + d - 2d \cos \beta_{lj} \\ &= 2d(1 - \cos \beta_{lj}) \end{aligned}$$

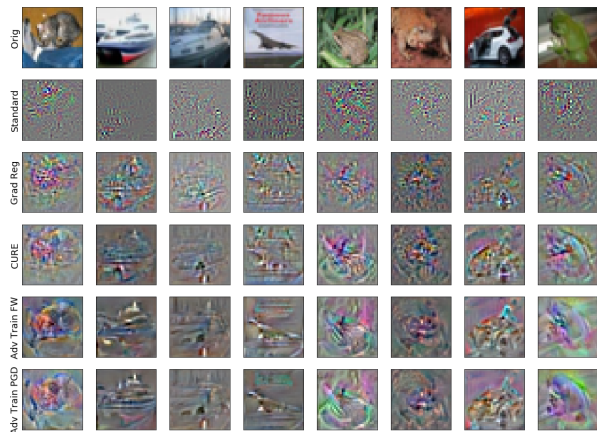
Rearranging the above expression, we obtain:

$$\begin{aligned} 1 - \cos \beta_{lj} &= \frac{\|s^l - s^j\|_2^2}{2d} = \frac{1}{2d} \sum_{i=1}^d (s_i^l - s_i^j)^2 \\ &= \frac{1}{2d} \sum_{i=1}^d 4 \cdot \mathbb{1}_{\{s_i^l \neq s_i^j\}} \\ &= \frac{2}{d} n_{lj} \end{aligned}$$

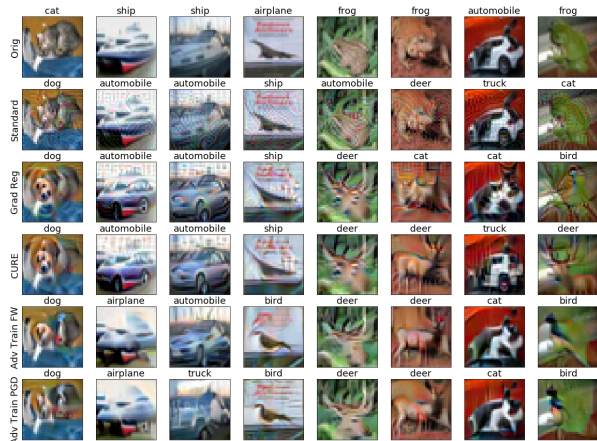
where $n_{lj} = \sum_{i=1}^d \mathbb{1}_{\{s_i^l \neq s_i^j\}}$ is the number of sign changes between the gradients $\nabla_{\delta^l} \ell(x + \delta^l, y)$ and $\nabla_{\delta^j} \ell(x + \delta^j, y)$. This concludes the proof. \square

Interpretability

We compare the quality of the saliency maps generated with a variety of regularized networks, in addition to adversarial perturbations that can serve as counterfactuals for explanations. Standard networks produce noisy saliency maps, as previously noted [11], and the higher level of robustness a network exhibits the more the network focuses on the object semantics as shown in Figure 5a. This is a good sign of lack of gradient obfuscation [30]. Using L^2 robust networks, the counterfactual images generated in Figure 5b by maximizing the loss align better with human perception for our method than for gradient and curvature regularized models.



(a) Saliency Maps.



(b) Adversarial Perturbations.

Figure 5: Saliency maps and PGD(20) untargeted adversarial attacks on the loss for sample examples from CIFAR-10 test set. FW-AT achieves more realistic-looking adversarial perturbations and improves saliency map quality.

Acknowledgements

Research was sponsored by the United States Air Force Research Laboratory and the United States Air Force Artificial Intelligence Accelerator and was accomplished under Cooperative Agreement Number FA8750-19-2-1000. The views and conclusions contained in this document are those of the authors and should not be interpreted as representing the official policies, either expressed or implied, of the United States Air Force or the U.S. Government. The U.S. Government is authorized to reproduce and distribute reprints for Government purposes notwithstanding any copyright notation herein.

References

- [1] Zeyuan Allen-Zhu, Yuanzhi Li, and Zhao Song. A convergence theory for deep learning via over-parameterization. In *ICML*, 2019. 5
- [2] Maksym Andriushchenko, Francesco Croce, Nicolas Flammarion, and Matthias Hein. Square attack: a query-efficient black-box adversarial attack via random search. In *ECCV*, 2020. 6
- [3] Anish Athalye, Nicholas Carlini, and David Wagner. Obfuscated gradients give a false sense of security: Circumventing defenses to adversarial examples. In *ICML*, 2018. 1, 2
- [4] Sebastian Bach, Alexander Binder, Gregoire Montavon, Frederick Klauschen, Klaus-Robert Muller, and Wojciech Samek. On pixel-wise explanations for non-linear classifier decisions by layer-wise relevance propagation. *PLoS one*, 10(7), 2015. 1, 5
- [5] Dimitri P. Bertsekas. *Nonlinear Programming*. Athena Scientific, 1999. 5
- [6] Yuan Cao and Quanquan Gu. Generalization error bounds of gradient descent for learning over-parameterized deep relu networks. In *AAAI*, 2020. 5
- [7] Chun-Hao Chang, Elliot Creager, Anna Goldenberg, and David Duvenaud. Explaining image classifiers by counterfactual generation. In *ICLR*, 2019. 3
- [8] Jinghui Chen, Dongruo Zhou, Jinfeng Yi, and Quanquan Gu. A frank-wolfe framework for efficient and effective adversarial attacks. In *Thirty-Fourth AAAI Conference on Artificial Intelligence*, 2020. 1, 3, 5
- [9] Amit Dhurandhar, Pin-Yu Chen, Ronny Luss, Chun-Chen Tu, Paishun Ting, Karthikeyan Shanmugam, and Payel Das. Explanations based on the missing: Towards contrastive explanations with pertinent negatives. In *NeurIPS*, 2019. 1
- [10] Logan Engstrom, Andrew Ilyas, Shibani Santurkar, and Dimitris Tsipras. Robustness (python library), 2019. 6
- [11] Christian Etmann, Sebastian Lunz, Peter Maass, and Carola-Bibiane Schonlieb. On the connection between adversarial robustness and saliency map interpretability. In *ICML*, 2019. 1, 5, 10
- [12] M. Frank and P. Wolfe. An algorithm for quadratic programming. *Naval research logistics quarterly*, 3:95–110, 1956. 3
- [13] Ian J. Goodfellow, Jonathon Shlens, and Christian Szegedy. Explaining and harnessing adversarial examples. In *International Conference on Learning Representations*, 2015. 1, 3
- [14] Chuan Guo, Jacob R. Gardner, Yurong You, Andrew Gordon Wilson, and Kilian Q. Weinberger. Simple black box adversarial attacks. In *ICML*, 2019. 1, 6
- [15] Andrew Ilyas, Shibani Santurkar, Dimitris Tsipras, Logan Engstrom, Brandon Tran, and Aleksander Madry. Adversarial examples are not bugs, they are features. In *NeurIPS 2019*, 2019. 1, 2
- [16] Martin Jaggi. Revisiting frank-wolfe: Projection-free sparse convex optimization. In *ICML*, pages 427–435, 2013. 3
- [17] Amir-Hossein Karimi, Gilles Barthe, Borja Balle, and Isabel Valera. Model-agnostic counterfactual explanations for sequential decisions. In *AISTATS*, 2020. 3

- [18] Alexey Kurakin, Ian J. Goodfellow, and Samy Bengio. Adversarial machine learning at scale. In *International Conference on Learning Representations*, 2017. 1
- [19] Simon Lacoste-Julien. Convergence rate of frank-wolfe for non-convex objectives. In *arXiv: 1607.00345*, 2016. 4, 5
- [20] Y. LeCun, Y. Bengio, and G. Hinton. Deep Learning. *Nature*, 521(7533):436–444, 2015. 1
- [21] Q. Vera Liao, Daniel Gruen, and Sarah Miller. Questioning the ai: Informing design practices for explainable ai user experiences. In *Conference on Human Factors in Computing Systems*, 2020. 5
- [22] C. Todd Lopez. *DOD Adopts 5 Principles of Artificial Intelligence Ethics*, 2020. 1
- [23] Chunchuan Lyu, Kaizhu Huang, and Ha-Ning Liang. A unified gradient regularization family for adversarial examples. In *IEEE International Conference on Data Mining (ICDM)*, 2015. 2, 7
- [24] Aleksander Madry, Aleksandar Makelov, Ludwig Schmidt, Dimitris Tsipras, and Adrian Vladu. Towards deep learning models resistant to adversarial attacks. In *International Conference on Learning Representations*, 2018. 1, 2, 6, 9
- [25] Microsoft. *Microsoft AI principles*, 2019. 1
- [26] Seyed-Mohsen Moosavi-Dezfooli, Jonathan Uesato, Alhussein Fawzi, and Pascal Frossard. Robustness via curvature regularization, and vice versa. In *IEEE Conference on Computer Vision and Pattern Recognition*, 2019. 1, 2, 5, 6, 7, 9
- [27] Ramaravind K. Mothilal, Amit Sharma, and Chenhao Tan. Explaining machine learning classifiers through diverse counterfactual explanations. In *Conference on Fairness, Accountability, and Transparency*, 2020. 3
- [28] Nicolas Papernot, Patrick McDaniel, Ian Goodfellow, Somesh Jha, Z. Berkay Celik, and Ananthram Swami. Practical black-box attacks against machine learning. In *arXiv:1602.02697v4*, 2017. 2
- [29] Sundar Pichai. *AI at Google: our principles*, 2018. 1
- [30] Chongli Qin, James Martens, Sven Gowal, Dilip Krishnan, Krishnamurthy Dvijotham, Alhussein Fawzi, Soham De, Robert Stanforth, and Pushmeet Kohli. Adversarial robustness through local linearization. In *NeurIPS*, 2019. 2, 5, 7, 10
- [31] Jarrid Rector-Brooks, Jun-Kun Wang, and Barzan Mozafari. Revisiting projection-free optimization for strongly convex constraint sets. In *AAAI*, 2019. 4, 5
- [32] Marco Ribeiro, Sameer Singh, and Carlos Guestrin. why should i trust you? explaining the predictions of any classifier. In *ACM SIGKDD Intl. Conference on Knowledge Discovery and Data Mining*, 2016. 1
- [33] Andrew Slavin Ros and Finale Doshi-Velez. Improving the adversarial robustness and interpretability of deep neural networks by regularizing their input gradients. In *AAAI Conference on Artificial Intelligence*, 2018. 1, 2, 7, 9
- [34] Pouya Samangouei, Ardavan Saeedi, Liam Nakagawa, and Nathan Silberman. Explaingan: Model explanation via decision boundary crossing transformations. In *ECCV*, 2018. 3
- [35] Shibani Santurkar, Andrew Ilyas, Dimitris Tsipras, Logan Engstrom, Brandon Tran, and Aleksander Madry. Image synthesis with a single (robust) classifier. In *NeurIPS*, 2019. 6
- [36] Shibani Santurkar, Dimitris Tsipras, Andrew Ilyas, and Aleksander Madry. How does batch normalization help optimization? In *NeurIPS*, 2018. 5
- [37] Uri Shaham, Yutaro Yamada, and Sahand Negahban. Understanding adversarial training: Increasing local stability of supervised models through robust optimization. *Neurocomputing*, 2018. 1
- [38] Shubham Sharma, Jette Henderson, and Joydeep Ghosh. Certifai: A common framework to provide explanations and analyse the fairness and robustness of black-box models. In *AIS*, 2020. 5
- [39] Dimitris Tsipras, Shibani Santurkar, Logan Engstrom, Alexander Turner, and Aleksander Madry. Robustness may be at odds with accuracy. In *International Conference on Learning Representations*, 2019. 1, 3, 5, 6
- [40] Jonathan Uesato, Brendan O’Donoghue, Aaron van den Oord, and Pushmeet Kohli. Adversarial risk and the dangers of evaluating against weak attacks. In *ICML*, 2018. 1, 2, 6
- [41] Sandra Wachter, Brent Mittelstadt, and Chris Russell. Counterfactual explanations without opening the black box: Automated decisions and the gdpr. *Harvard Journal of Law & Technology*, 31(2), 2018. 1, 3, 5
- [42] Yisen Wang, Xingjun Ma, James Bailey, Jinfeng Yi, Bowen Zhou, and Quanquan Gu. On the convergence and robustness of adversarial training. In *ICML*, 2019. 3
- [43] Tsui-Wei Weng, Huan Zhang, Hongge Chen, Zhao Song, Cho-Jui Hsieh, Duane Boning, Inderjit S. Dhillon, and Luca Daniel. Towards fast computation of certified robustness for relu networks. In *ICML*, 2018. 1
- [44] Matthew D. Zeiler and Rob Fergus. Visualizing and understanding convolutional networks. In *European Conference on Computer Vision*, 2014. 5
- [45] Difan Zou and Quanquan Gu. An improved analysis of training over-parameterized deep neural networks. In *NeurIPS*, 2019. 5